Bulletin of the Seismological Society of America, Vol. 86, No. 1B, pp. S19–S36, February 1996

Co-Seismic Displacements of the 1994 Northridge, California, Earthquake

by K. W. Hudnut, Z. Shen, M. Murray, S. McClusky, R. King, T. Herring, B. Hager, Y. Feng, P. Fang, A. Donnellan, and Y. Bock

Abstract The 17 January 1994 Northridge, California, earthquake significantly deformed the Earth's crust in the epicentral region. Displacements of 66 survey stations determined from Global Positioning System (GPS) observations collected before and after the earthquake show that individual stations were uplifted by up to 417 ± 5 mm and displaced horizontally by up to 216 ± 3 mm. Using these displacements, we estimate parameters of a uniform-slip model. Fault geometry and slip are estimated independent of seismological information, using Monte Carlo optimization techniques that minimize the model residuals. The plane that best fits the geodetic data lies 1 to 2 km above the plane indicated by aftershock seismicity. Modeling for distributed slip on a coplanar, yet larger model fault indicates that a high-slip patch occurred up-dip and northwest of the mainshock hypocenter and that less than 1 m of slip occurred in the uppermost 5 km of the crust. This finding is consistent with the lack of clear surface rupture and with the notion that the intersection with the fault that ruptured in 1971 formed the up-dip terminus of slip in the Northridge earthquake. Displacements predicted by either of these simple models explain most of the variance in the data within 50 km of the epicenter. On average, however, the scatter of the residuals is twice the data uncertainties, and in some areas, there is significant systematic misfit to either model. The co-seismic contributions of aftershocks are insufficient to explain this mismatch, indicating that the source geometry is more complicated than a single rectangular plane.

Introduction

The M_w = 6.7 17 January 1994 Northridge earthquake (USGS and SCEC, 1994) produced measurable co-seismic displacements over a large area (approximately 4000 km^2) including much of the San Fernando Valley and adjacent mountainous areas. Over the region of largest slip on the fault plane, the Earth's surface was pressed into an asymmetric dome-shaped uplift, skewed toward the NNE. Over the uplifted region, the largest horizontal displacements also occurred, with displacement outward from the apex of the dome. The significant NNE-oriented shortening at the NNE and SSW margins of the domed area indicate the net compression that occurred between the hanging wall and footwall of the thrust fault that ruptured.

We have used Global Positioning System (GPS) geodetic data to quantify the static displacement field associated with the earthquake and its aftershocks. In this study, we sampled the displacement field at 66 stations (documented in Tables 1 and A1) with GPS-derived vectors measured with 1-sigma errors ranging 3 to 42 mm (east–west), 3 to 25 mm (north–south), and 3 to 90 mm (vertical). Our estimates are based on station positions measured within 15 months prior to and 1 month following the earthquake. In our analysis, we corrected for secular velocities at all of the stations by spatially interpolating between velocities estimated previously for 15 stations, using measurements spanning 5 or more years.

From the set of co-seismic displacement vectors we determined, we modeled the earthquake source using previously established methods based on the elastic dislocation theory. First, we estimated the dislocation source that could best explain the geodetic data with a single uniform-slip dislocation following the nonlinear optimization approach of Murray *et al.* (1994) and using a single rectangular dislocation in a homogeneous half-space. We then estimated the spatial distribution of slip on a larger (yet coplanar) fault surface following the singular value decomposition inversion approach implemented by Larsen (1991). This modeling is secondary to the data portions of this article and should be viewed in the context of other studies of the earthquake's source (Wald and Heaton, 1994b; Dreger, 1994; Shen *et al.*, this issue; Wald *et al.*, this issue). The models presented here interpret these GPS data independent of other information. Wald *et al.* (this issue) combine these GPS results with other data to estimate a more comprehensive source model.

Table 1

GPS Displacements and Model Residuals (displacements and residuals are in millimeters; errors are 1-sigma; component and vector "nres" values are normalized residuals)

Station			Uniform		Variable				Uniform		Variable		Correl.			Uniform		Variable		Uniform	Variable
ID	East	E_err	E_res	E_nres	E_res	E_nres	North	N_err	N_res	N_nres	N_res	N_nres	NE	Up	U_err	U_res	U_nres	U_res	U_nres	NRES	NRES
0094	39.8	4.9	10.7	2.18	11.1	2.27	56.2	5.6	19.1	3.41	16.4	2.93	−0.124	−32.8	32.0	−19.8	0.62	−23.7	0.74	2.37	2.18
0141	−14.8	19.8	10.1	0.51	12.6	0.64	−39.0	8.9	5.8	0.65	9.5	1.07	0.457	−51.0	48.7	−40.3	0.83	−38.5	0.79	0.68	0.85
0618	−5.7	3.9	−7.2	1.85	−6.6	1.69	−0.2	4.2	6.2	1.48	8.2	1.95	−0.121	7.1	19.4	8.0	0.41	8.0	0.41	1.39	1.51
0701	−1.9	3.5	0.7	0.20	2.7	0.77	25.8	3.7	1.6	0.43	0.7	0.19	−0.014	3.3	13.8	9.4	0.68	9.0	0.65	0.48	0.59
0702	−0.1	3.5	−2.5	0.71	−2.3	0.66	2.0	3.8	1.2	0.32	2.3	0.61	0.064	−23.4	14.6	−20.6	1.41	−20.5	1.40	0.93	0.96
0703	21.7	4.2	7.7	1.83	8.4	2.00	25.6	4.0	10.7	2.67	10.7	2.67	0.118	−11.1	16.0	−7.9	0.49	−8.7	0.54	1.89	1.95
0704	−31.5	3.1	−19.9	6.42	−9.4	3.03	−58.0	3.1	−18.2	5.87	2.2	0.71	−0.090	14.0	6.1	23.1	3.79	24.4	4.00	5.48	2.93
0705	13.5	4.5	15.3	3.40	16.5	3.67	0.6	4.2	2.2	0.52	3.7	0.88	0.098	−46.8	19.4	−45.8	2.36	−45.7	2.36	2.41	2.57
07CG	−0.8	4.9	0.6	0.12	2.7	0.55	28.2	5.8	2.8	0.48	0.3	0.05	−0.050	−8.7	34.1	−4.3	0.13	−3.7	0.11	0.30	0.33
07CI	2.4	20.1	2.1	0.10	2.5	0.12	9.5	9.5	3.7	0.39	4.7	0.49	0.423	−62.1	54.2	−59.2	1.09	−59.3	1.09	0.67	0.70
07DI	7.4	19.3	4.2	0.22	3.5	0.18	5.5	8.1	3.2	0.40	4.8	0.59	0.523	5.7	46.9	9.4	0.20	9.0	0.19	0.28	0.37
07EH	−5.7	27.8	−15.4	0.55	−17.6	0.63	3.1	19.2	5.2	0.27	6.5	0.34	0.630	−91.8	67.7	−87.9	1.30	−88.9	1.31	0.83	0.86
07FI	−4.4	5.0	−0.1	0.02	1.7	0.34	−7.6	5.1	−2.3	0.45	−0.1	0.02	−0.281	5.2	24.2	8.7	0.36	9.2	0.38	0.33	0.29
1201	3.4	3.6	3.5	0.97	4.4	1.22	2.9	3.6	−2.3	0.64	−1.8	0.50	0.042	−22.0	13.1	−20.8	1.59	−20.7	1.58	1.14	1.19
2131	6.1	3.7	4.1	1.11	4.7	1.27	−20.1	3.5	−1.5	0.43	3.1	0.89	−0.279	−20.0	11.9	−16.0	1.34	−15.7	1.32	1.04	1.17
56_Z	−5.5	29.6	−4.8	0.16	−3.9	0.13	2.2	8.2	−6.1	0.74	−5.7	0.70	0.370	80.6	73.5	82.8	1.13	82.9	1.13	0.79	0.77
ALPN	−14.0	32.7	−5.7	0.17	−3.8	0.12	−3.7	19.6	5.7	0.29	8.5	0.43	0.539	−21.8	72.6	−20.2	0.28	−20.0	0.28	0.25	0.30
BREN	−5.2	3.5	−3.5	1.00	0.3	0.09	42.3	3.4	1.1	0.32	−3.5	1.03	−0.047	−35.9	10.5	−25.0	2.38	−24.2	2.30	1.50	1.46
BURB	9.7	4.0	−4.3	1.07	−10.4	2.60	3.7	4.3	4.2	0.98	8.2	1.91	−0.105	−72.4	20.0	−70.3	3.52	−77.8	3.89	2.20	2.92
CAHA	8.2	3.7	−3.3	0.89	−8.7	2.35	9.4	4.0	8.6	2.15	12.5	3.12	0.009	6.2	17.2	9.1	0.53	2.7	0.16	1.38	2.26
CALA	41.2	3.1	11.0	3.55	9.6	3.10	78.8	3.1	8.7	2.81	0.0	0.00	−0.047	−2.6	5.7	19.4	3.40	28.5	5.00	3.27	3.40
CATO	30.8	3.2	3.2	1.00	1.4	0.44	45.7	3.2	8.1	2.53	5.1	1.59	0.043	−10.0	7.5	−0.4	0.05	−0.1	0.01	2.72	1.65
CHAT	−110.0	3.3	−22.3	6.76	−8.9	2.70	35.7	3.2	27.1	8.47	6.9	2.16	−0.035	154.0	8.2	−33.1	4.04	−39.7	4.84	6.68	3.43
CHRN	−96.0	5.0	13.5	2.70	−6.6	1.32	47.6	5.3	21.7	4.09	−21.3	4.02	−0.215	134.7	26.4	−4.2	0.16	1.1	0.04	2.83	2.44
DUMP	46.6	11.4	25.9	2.27	24.1	2.11	46.7	6.3	16.3	2.59	13.4	2.13	0.467	−22.7	36.9	−17.1	0.46	−16.7	0.45	2.01	1.75
GLEN	9.1	3.5	−3.8	1.09	−8.8	2.51	−8.6	3.4	−6.9	2.03	−4.3	1.26	−0.226	−5.6	12.8	−2.5	0.20	−6.5	0.51	1.33	1.65
HAP2	−20.7	3.1	−9.2	2.97	−5.0	1.61	13.4	3.1	7.1	2.29	4.5	1.45	0.005	12.7	6.3	15.3	2.43	11.7	1.86	2.58	1.65
HAPY	−42.6	3.2	−26.8	8.38	−23.6	7.37	22.3	3.2	14.8	4.62	12.2	3.81	0.101	12.7	7.9	14.4	1.82	11.7	1.48	5.62	4.87
HOPP	−17.5	3.2	−13.0	4.06	−11.7	3.66	6.3	3.2	6.1	1.91	7.1	2.22	0.148	15.1	7.3	19.0	2.60	19.5	2.67	3.00	2.91
JPLM	6.6	3.0	−0.3	0.10	−1.5	0.50	−7.3	3.0	−5.9	1.97	−4.6	1.53	−0.027	−1.8	3.1	2.2	0.71	1.9	0.61	1.21	1.00
LOVE	−84.6	3.1	−85.2	27.48	−84.3	27.19	−44.7	3.1	−19.8	6.39	−10.2	3.29	−0.022	−68.8	5.5	−61.6	11.20	−60.3	10.96	17.53	17.03
MALI	31.4	4.5	7.9	1.76	4.8	1.07	59.2	5.2	6.8	1.31	−1.8	0.35	−0.074	−18.5	30.9	−6.6	0.21	−2.8	0.09	1.27	0.65
MAND	2.9	3.5	2.3	0.66	7.2	2.06	57.5	3.7	9.4	2.54	2.3	0.62	−0.006	−17.7	13.9	−3.9	0.28	−2.5	0.18	1.52	1.25
MAYO	12.6	3.7	−1.7	0.46	−1.0	0.27	5.9	4.0	13.9	3.47	0.6	0.15	−0.050	5.3	17.0	−2.9	0.17	−6.1	0.36	2.03	0.27
MLND	6.8	4.7	1.5	0.32	6.9	1.47	33.6	5.5	2.1	0.38	−2.6	0.47	−0.021	3.6	31.0	9.4	0.30	4.5	0.15	0.34	0.89
MULH	6.1	3.4	−6.0	1.76	−3.5	1.03	64.1	3.3	−1.4	0.42	−14.3	4.33	−0.054	−18.8	9.8	−1.9	0.19	9.5	0.97	1.05	2.63
NEWH	−98.6	13.7	−91.2	6.66	−65.6	4.79	47.3	6.5	−6.9	1.06	−18.3	2.82	0.479	249.8	32.5	179.9	5.54	153.5	4.72	5.04	4.21
NIKE	1.7	3.5	−4.5	1.29	1.4	0.40	59.9	3.5	13.6	3.89	3.4	0.97	−0.017	−39.0	11.8	−29.6	2.51	−26.7	2.26	2.77	1.44
NORT	34.8	3.3	4.8	1.45	5.0	1.52	−58.8	3.3	−19.4	5.88	1.1	0.33	−0.338	213.2	8.1	−40.2	4.96	−38.0	4.69	4.52	2.85
N_49	9.3	34.4	6.1	0.18	9.1	0.26	55.0	24.5	1.2	0.05	−8.0	0.33	0.710	−29.2	87.5	−15.9	0.18	−11.8	0.13	0.15	0.25
OJAI	−0.8	5.0	−0.1	0.02	1.3	0.26	−1.1	7.2	−2.7	0.38	−1.9	0.26	−0.260	−34.2	35.9	−31.8	0.89	−31.7	0.88	0.56	0.55
PACO	86.5	3.2	0.5	0.16	−3.9	1.22	−13.4	3.1	−1.5	0.48	−2.7	0.87	−0.032	64.2	6.5	16.1	2.48	−8.4	1.29	1.46	1.14
PARK	−5.2	3.4	7.1	2.09	9.5	2.79	−18.9	3.4	−5.0	1.47	−1.6	0.47	0.074	−32.9	10.2	−29.1	2.85	−28.4	2.78	2.21	2.29

Table 1
Continued

Station ID	East	E_err	Uniform E_res	Uniform E_nres	Variable E_res	Variable E_nres	North	N_err	Uniform N_res	Uniform N_nres	Variable N_res	Variable N_nres	Correl. NE	Up	U_err	Uniform U_res	Uniform U_nres	Variable U_res	Variable U_nres	Uniform NRES	Variable NRES
PEAR	12.5	3.2	16.2	5.06	17.7	5.53	4.4	3.2	8.0	2.50	9.8	3.06	0.095	−13.7	7.2	−12.5	1.74	−12.3	1.71	3.41	3.78
PELN	−14.9	27.3	0.7	0.03	3.2	0.12	−35.0	19.2	−4.8	0.25	0.0	0.00	0.619	37.2	69.4	40.9	0.59	41.4	0.60	0.37	0.35
PICO	−116.2	3.2	15.0	4.69	12.8	4.00	162.2	3.1	−4.4	1.42	0.0	0.00	0.029	388.5	6.7	−21.3	3.18	−16.6	2.48	3.37	2.72
PVEP	−1.8	3.0	−1.9	0.63	−0.6	0.20	14.1	3.0	−0.2	0.07	−1.3	0.43	−0.002	0.9	3.1	2.0	0.65	2.2	0.71	0.52	0.49
PVER	5.3	3.4	5.2	1.53	6.5	1.91	19.6	3.5	5.3	1.51	4.2	1.20	0.030	34.7	12.2	35.8	2.93	36.0	2.95	2.10	2.14
RESE	196.8	3.2	−11.6	3.62	0.1	0.03	−5.7	3.2	−19.7	6.16	0.5	0.16	−0.323	333.0	7.2	−21.7	3.01	−7.0	0.97	4.48	0.57
SAFE	−141.4	3.1	−9.6	3.10	−11.9	3.84	163.0	3.1	−3.2	1.03	1.0	0.32	0.004	416.6	5.0	5.6	1.12	10.2	2.04	1.99	2.52
SAFR	−130.1	3.4	1.7	0.50	−0.8	0.24	161.5	3.4	−4.7	1.38	−0.8	0.24	−0.032	393.7	10.5	−16.8	1.60	−11.3	1.08	1.25	0.65
SATI	76.2	3.2	13.6	4.25	12.7	3.97	−27.2	3.3	−7.0	2.12	−11.0	3.33	0.033	47.0	8.5	6.3	0.74	−24.4	2.87	2.78	3.42
SNPA	−13.1	3.2	−9.1	2.84	−6.7	2.09	4.9	3.3	2.0	0.61	2.0	0.61	0.112	−8.9	8.5	−5.3	0.62	−5.7	0.67	1.72	1.32
SPHI	−3.8	3.7	−3.1	0.84	−1.7	0.46	16.1	3.9	2.2	0.56	1.4	0.36	−0.100	−9.2	16.5	−7.6	0.46	−7.4	0.45	0.64	0.42
TUNA	36.0	3.2	21.7	6.78	21.9	6.84	83.4	3.1	15.0	4.84	2.0	0.65	−0.010	−27.3	7.0	−8.4	1.20	−0.4	0.06	4.86	3.97
U145	−53.4	5.0	−28.2	5.64	−18.3	3.66	10.8	4.9	−4.5	0.92	−9.9	2.02	−0.135	39.8	23.0	31.7	1.38	30.4	1.32	3.39	2.53
UCLA	−4.3	3.4	−2.6	0.76	0.3	0.09	50.7	3.4	20.0	5.88	19.0	5.59	−0.009	−29.0	11.0	−19.8	1.80	−22.3	2.03	3.58	3.43
USC2	4.4	4.8	4.1	0.85	3.9	0.81	17.7	5.7	8.7	1.53	10.3	1.81	−0.083	−27.5	32.5	−23.2	0.71	−24.2	0.74	1.09	1.22
VDGO	16.8	3.8	−0.6	0.16	−5.7	1.50	−5.0	4.0	−1.2	0.30	0.2	0.05	0.037	−23.9	18.1	−21.8	1.20	−25.3	1.40	0.72	1.18
VENI	6.4	3.8	8.7	2.29	11.0	2.89	27.1	4.0	1.1	0.27	−0.7	0.18	0.024	−22.3	17.9	−16.7	0.93	−16.4	0.92	1.44	1.76
W304	−0.6	4.9	−0.9	0.18	1.5	0.31	16.7	6.9	13.9	2.01	14.3	2.07	−0.196	−13.9	30.2	−11.0	0.36	−11.4	0.38	1.19	1.23
WARN	32.4	41.2	30.5	0.74	31.1	0.75	−4.5	18.4	6.3	0.34	9.1	0.49	0.342	0.1	88.3	2.1	0.02	2.2	0.02	0.47	0.52
WBCH	4.5	3.8	5.7	1.50	7.4	1.95	17.5	4.1	−1.7	0.41	−3.2	0.78	−0.010	−38.5	19.1	−35.6	1.86	−35.3	1.85	1.40	1.61
WHIT	−18.4	3.3	−20.2	6.12	−19.7	5.97	−21.9	3.3	−6.8	2.06	−2.7	0.82	0.054	−8.5	9.1	−4.4	0.48	−3.8	0.42	3.74	3.49
Z370	2.1	27.2	1.0	0.04	2.1	0.08	−37.5	19.2	−8.2	0.43	−0.3	0.02	0.589	0.1	71.0	6.2	0.09	6.6	0.09	0.25	0.07
Z786	50.1	17.2	3.7	0.22	−7.1	0.41	−3.6	5.7	7.7	1.35	8.9	1.56	0.160	20.9	26.0	6.0	0.23	−12.7	0.49	0.80	0.97

All Data:

	East	North	Up
Mean of ERR:	7.9	5.8	23.4
Std. Dev. of ERR:	9.2	4.8	21.6

All Data:

	Uniform	Variable	Uniform	Variable	Uniform	Variable	Uniform	Variable
Mean of NRES:	2.32	2.15	1.85	1.25	1.50	1.48	2.18	1.92
Standard deviation of NRES:	3.77	3.57	1.88	1.24	1.75	1.75	2.44	2.21
Excluding Station LOVE:								
Mean of NRES:	1.93	1.76	1.78	1.21	1.35	1.34	1.94	1.69
Standard deviation of NRES:	2.10	1.73	1.81	1.23	1.27	1.30	1.52	1.16

Note: For this analysis, the global stations ALGO, FAIR, KOKB, MADR, HART, YELL, YAR1, KOSG, TROM, WETT, SANT, TIDB, and DS1B were constrained to their ITRF'93 positions.

Data and Analysis

The GPS data used for our analysis were obtained in field surveys between October 1992 and February 1994 and from continuous observations at stations of the southern California permanent GPS geodetic array (PGGA) (Bock, 1993b) and the global tracking network overseen by the International GPS Service for Geodynamics (IGS) (Beutler and Brockmann, 1993). The accuracy with which a station's position can be estimated from each field survey is generally 5 to 15 mm for the horizontal coordinates and 10 to 30 mm for height (see Table 1, error columns), depending primarily on the number of days that station was observed and the length of each observation session. Most of the pre-earthquake and postearthquake data are from four distinct field projects, each of which has a different history of observations that is documented in Table A2 and Figure A1. A total of 534 occupations of 66 survey stations were made during 92 field sessions. These data were combined with global and regional continuously recorded GPS data covering 24 hours on the day of each field session.

We analyzed the data in two steps. In the first step, we used the GPS phase and pseudorange measurements to estimate station coordinates, satellite orbital parameters, and atmospheric delay corrections for each day of observation. For this step, we loosely constrained the coordinates and velocities of regional and global stations. In the second step, we combined the estimates and their covariance matrices from all of the days, applying position and velocity constraints to 13 globally distributed stations (listed in Table 1) to obtain a consistent solution for displacements at the epoch of the earthquake. For all of the experiments, we resolved integer-cycle ambiguities in the phase observations using the iterative technique described by Feigl *et al.* (1993). The two-step approach allowed us to distribute both the processing of the raw GPS observations and the combination of solutions among several groups, encouraging redundant and progressively improved analyses (see Table A2).

Figures 1 and 2 and Table 1 show our estimates of displacements for 66 GPS monuments within about 75 km of the Northridge epicenter. The uncertainties given in Table 1 and plotted in Figures 1 and 2 represent our best estimate of the 1-sigma error for each value or vector. These cannot be rigorously computed from the uncertainty in the GPS phase measurements because the error spectrum of these measurements is poorly understood. Rather, they are based on studies of short- and long-term repeatabilities for a subset of station position estimates from this analysis and the set for southern California between 1986 and 1992 (Feigl *et al.*, 1993). These studies suggest that for short observation sessions (<5 hr), the formal uncertainties are roughly consistent with long-term repeatability; for longer single-day sessions (5 to 8 hr), the formal uncertainties should be increased by a factor of 2 to 3; and for sessions of 24 hr or more, the appropriate scale factor is 3 to 4. Since the present analysis includes data from observation sessions ranging from 2 to 24 hr, a simple scaling of the formal uncertainties to achieve a chi-square of unity for the long-term scatter of estimates is inappropriate. The simplest approach, which we have adopted, is to add a constant value ($[3\ \text{mm}]^2$) to the variance estimated for each coordinate in the solution.

We are able to check the validity of our weighting by examining the estimated displacements of stations sufficiently far from the epicenter that we expect small errors in their modeled displacements. If we adopt the arbitrary criteria that these stations should have model-predicted displacements less than 10 mm in all components, and estimated uncertainties less than 10 mm in the horizontal and 40 mm in the vertical components, then 12 stations are available for analysis. One of these stations, HOPP, has a 4-sigma residual in its east component (-13 ± 3 mm), a result that may be related to unmodeled motion on a second fault plane (discussed below). A second station, PEAR, has a 5-sigma residual in the east (16 ± 3 mm) that is not yet understood. For the remaining 10 stations (whose names are italicized in Table 1), the values of the square root of the reduced chi-square (nrms) for the east, north, and vertical residuals are 1.5, 1.0, and 1.2, respectively. From this we conclude that the uncertainties given in Table 1 are reasonable estimates of the 1-sigma errors for most stations.

Another concern arises from the small number of independent measurements for many stations (Fig. A1). For monuments with only one or two measurements in either the period before or after the earthquake, there is significant chance of undetected error. Such an error could arise in either the observations (e.g., by receiver malfunction, by improperly positioning the antenna over the survey monument, or by mis-measuring the antenna height) or the analysis (e.g., improperly repairing cycle slips).

All pre-earthquake data we used were collected within 15 months of the earthquake. Since the relative interseismic motions of most of the stations are small or well known, there is little error introduced by mismodeling these motions. The assumed velocities for the stations involved in this study (Table A1) were interpolated using 15 well-determined secular velocities and a simple model for slip on the San Andreas fault system (Feigl *et al.*, 1993). We believe that the velocity errors for the stations we used are less than 3 mm/yr.

Modeling

We used two methods to model the measured displacements. First, we applied an extension of the Monte Carlo technique following Murray *et al.* (1994), an approach that is well suited to finding the single-dislocation model that best fits the geodetic data and that is independent of seismological and geological information. To the extent that the inherent simplifying assumptions are valid, the result of this method points out that the geodetic data are best fit by slip on a plane that lies 1 to 2 km above the aftershock plane, northwest and up-dip of the mainshock hypocenter. Second, by inversion of the displacement data, we estimated variable

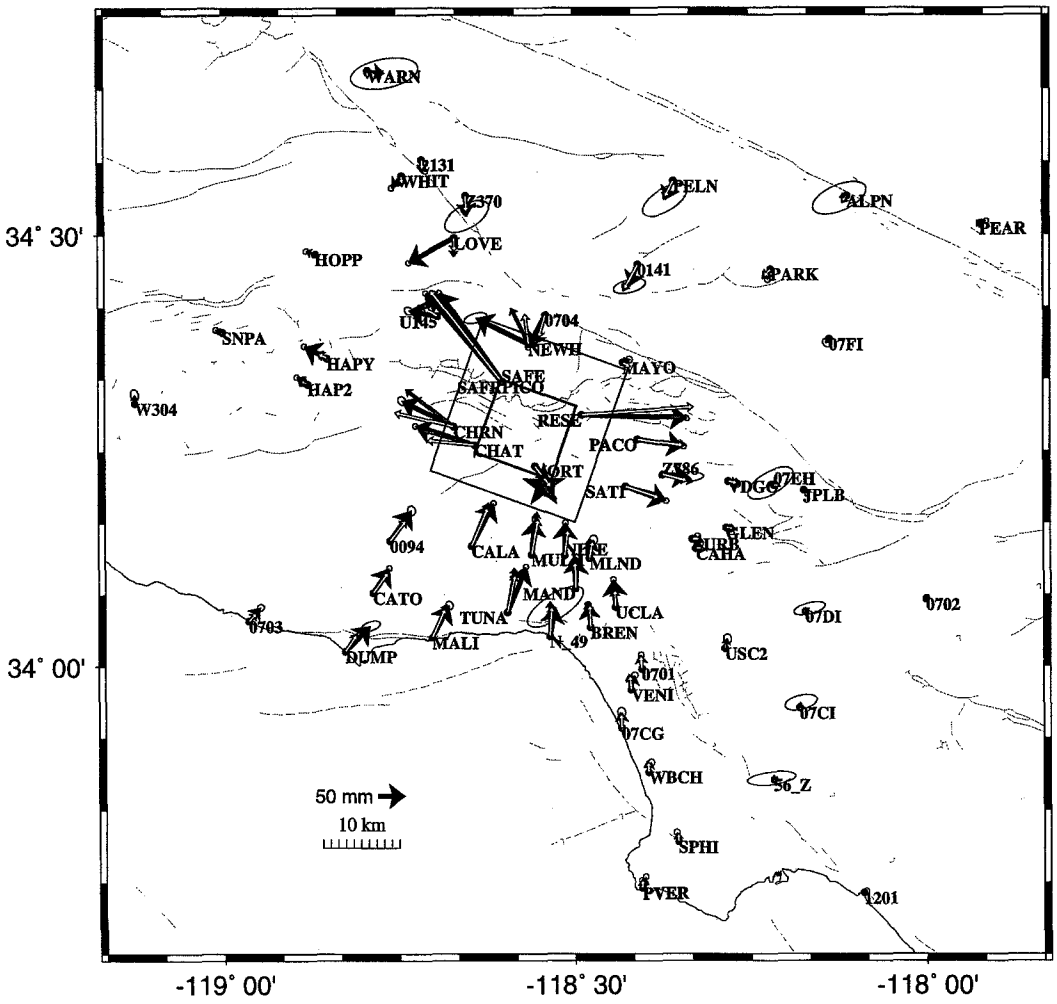

Figure 1. Measured displacements associated with the Northridge earthquake. Station locations are indicated by gray circles (and identified by a 4-character I.D. for reference to the tables). Horizontal displacement is shown by a heavy black vector and corresponding 1-sigma ellipse. Uniform-slip model vectors are shown in white; variable slip model is shown in gray.

slip on an enlarged and coplanar model fault plane. Neither approach led to statistically adequate fits to the GPS data, yet we limited ourselves to this class of models for the sake of simplicity. Also, because we had no unambiguous, objective basis to discard outliers, all of the GPS measurements were included in both modeling approaches, despite our recognition that certain stations clearly could not be fit well with these simple source models.

Both approaches are based on the elastic dislocation theory, which can be used to compute the displacements at a given point on the ground surface from a slip distribution model (e.g., Steketee, 1958; Chinnery, 1961; Savage and Hastie, 1966; Mansinha and Smylie, 1971; Okada, 1985). Both our forward and inverse modeling approaches incorporated a combination of algorithms from these references. The model geometry is displayed in Figures 1, 2 and 3, where we indicate the map view and cross-section geometry of the model fault surfaces. Modeled displacements are shown in Figures 1 and 2, and the residuals between the observations and each of the two models are given in Table 1 and Figure 7.

Nonlinear Optimization Method

We first estimated the best model with uniform slip on a single rectangular fault. This simple model is described by nine parameters that give the location, orientation, and dimensions of the dislocation plane, as well as the slip vector on that plane (see Table 2). We used nonlinear optimization methods, based on extensions of the Monte Carlo technique, to randomly vary the fault geometry and estimate the slip vector until the model with the smallest sum-squared residuals (χ^2) was found. This method provides a fault model that, on average, shows where the slip is concentrated at depth, but the assumption of uniform slip on a simple rectangle is clearly an oversimplification of the actual slip distribution.

We used the following procedures and assumptions,

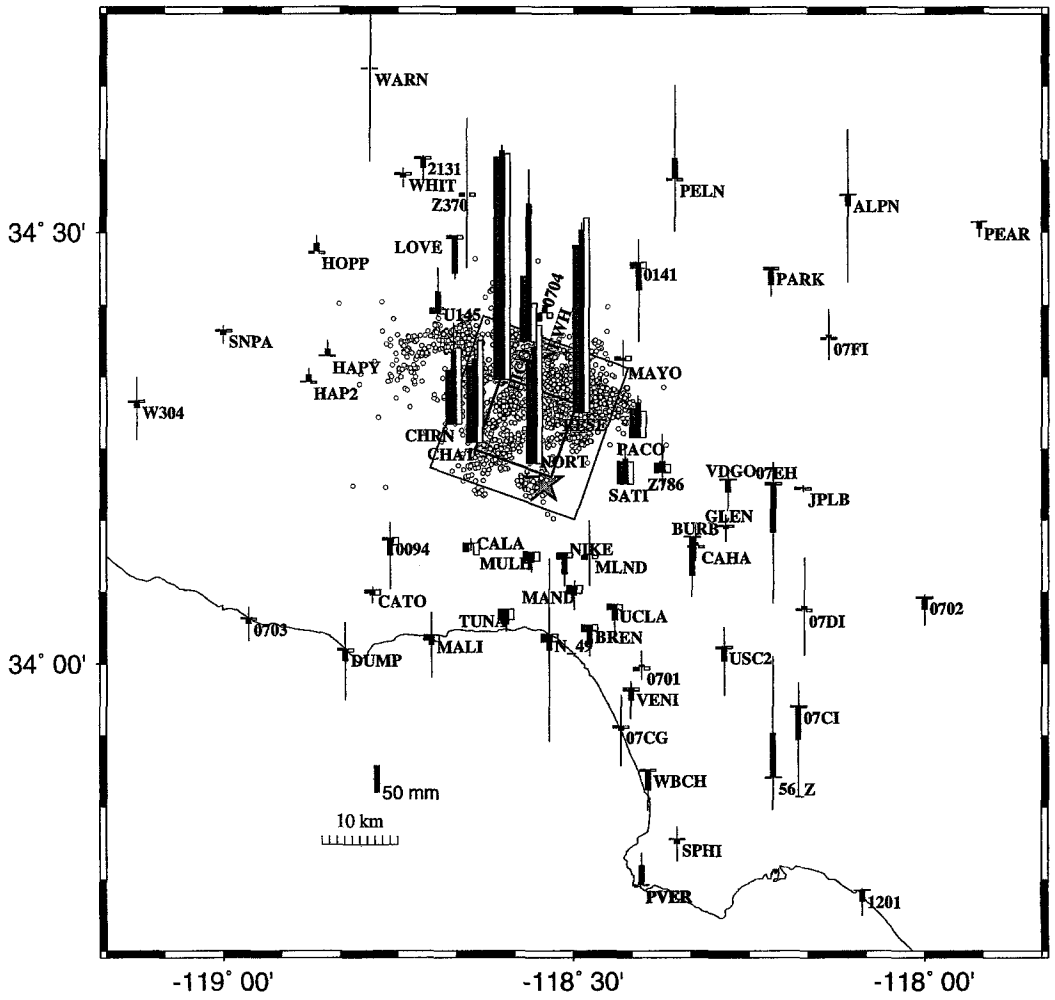

Figure 2. Measured and modeled vertical displacements at the GPS stations. Measured vertical displacements are shown by the central black column at each station, and the 1-sigma error is indicated by a vertical line. Uniform-slip model columns are shown in white; variable slip model is shown in gray.

Table 2
Model Parameters for Optimal Single-Dislocation Source Model and Its 95% Confidence Limits

Parameter	Optimal Model	95% Range	
		Low	High
Strike (deg)	109.56	100.53	118.77
Dip (deg)	40.96	38.17	43.65
Width (km)	13.28	9.35	17.12
Length (km)	10.51	6.28	13.11
Centroid depth (km)	10.07	9.00	11.34
Centroid latitude (deg)	34.2753	34.2647	34.2834
Centroid longitude (deg)	−118.5674	−118.5605	−118.5762
Slip magnitude (m)	2.50	1.91	4.40
Slip rake (deg)	91.3	84.1	97.2
Moment (N-m)	1.05×10^{19}	0.93×10^{19}	1.19×10^{19}

based on Murray *et al.* (1994). Slip was assumed to be uniform on a single rectangular fault, with its top edge parallel to the Earth's surface and embedded in a homogeneous isotropic elastic half-space with rigidity = 30 GPa. The projection was polyconic, with east-north correlations neglected. While the modeling procedure could be improved mathematically by including the correlations, which are available from the GPS data analysis (Table 1), such a change would be unlikely to cause substantive changes in our results.

For the optimal model, $\chi^2 = 2082$ (with 198 data and estimating nine parameters), yielding an nrms residual of 3.32. To assess uncertainties in the model, we compared trial models to the optimal model using an F-ratio test (Draper and Smith, 1981). Table 2 gives the parameters for the optimal model (and its 95% confidence limits), and Table 1 and Figure 6 show the distribution of normalized residual values. We believe that the large nrms residual results primarily from using too simple a model and not necessarily from an underestimate of uncertainties in the displacements,

as discussed below. Nevertheless, this model explains 95% of the variance in the GPS data (for the null model, i.e., no deformation, $\chi^2 = 41{,}600$).

The plane estimated by this approach dips toward the SSW and indicates that the main slip concentration occurred up-dip and toward the northwest of the mainshock hypocenter. This plane is evidently not coplanar with the aftershocks. Figure 3 shows the model plane plotted in cross section with respect to relocated aftershocks from Mori *et al.* (1995). The model plane is nearly parallel to the seismicity plane, lying 1 to 2 km above it. At the hypocenter, the vertical distance from the hypocenter to the (projected) model plane is about 2 km, considerably greater than the stated error in hypocentral depth of 0.4 km. One possible explanation that has not yet been evaluated is that the hypocenter determination and GPS-based modeling approaches have different datums, causing a shift in apparent depth that is due mainly to differences in methods. However, it seems highly unlikely that so large a shift could occur from that alone. More importantly, our assumption of a uniform Poisson solid for the physical model may introduce inaccuracy. A similar discrepancy has been observed and discussed elsewhere (e.g., Ekstrom *et al.,* 1992; Stein and Ekstrom, 1992), in which case it was attributed to assuming a half-space in the presence of variable crustal rigidity surrounding the modeled fault. This possibility is also noted by Shen *et al.* (this issue) and treated in more detail there.

Singular Value Decomposition Inversion Method

To solve for the slip distribution on an assumed fault plane, we applied singular value decomposition (SVD) (e.g., Jackson, 1972; Menke, 1989). SVD is a matrix decomposition technique used to estimate parameters when the model space is poorly constrained by the data. This approach is often used in geodetic inversions for fault slip, since the data must be obtained at the surface and, therefore, poorly resolve slip at depth (Harris and Segall, 1987; Segall and Harris, 1987; Freymueller *et al.,* 1994; Hudnut and Larsen, 1993). The technique is equivalent to least squares when the number of singular values equals the number of unknown parameters. Using a lower number of singular values means that only those parts of the model that are well mapped by the data will be estimated.

This modeling approach assumes a fault geometry. We assumed the model fault to be coplanar with that estimated by our nonlinear optimization approach (Fig. 3). We roughly doubled the length and width dimensions and extended the model plane up-dip; we used the strike, dip, and location of the optimal plane (Table 2). We assumed the fault plane to be 20 by 26 km and specified it to be composed of 130 subfaults, each 2 by 2 km. The model fault plane extends to within 1 km of the ground surface, and the center point of this plane is located at a depth of 9.86 km. We inverted the GPS estimates of displacement vector components and their associated errors (from Table 1) to estimate the thrust and strike-slip components of slip on each subfault, as described by Larsen (1991) and Hudnut and Larsen (1993). The number of parameters estimated was 260, and the number of data was 198 (each displacement vector contains three components).

We employed no positivity or slip constraints, nor smoothing apart from that which occurs inherently in the SVD method of inversion. In SVD, when the eigenvalue matrix is truncated, a form of smoothing is implemented. In this case, the number of singular values chosen was 23, because this solution was within the range of most reasonable solu-

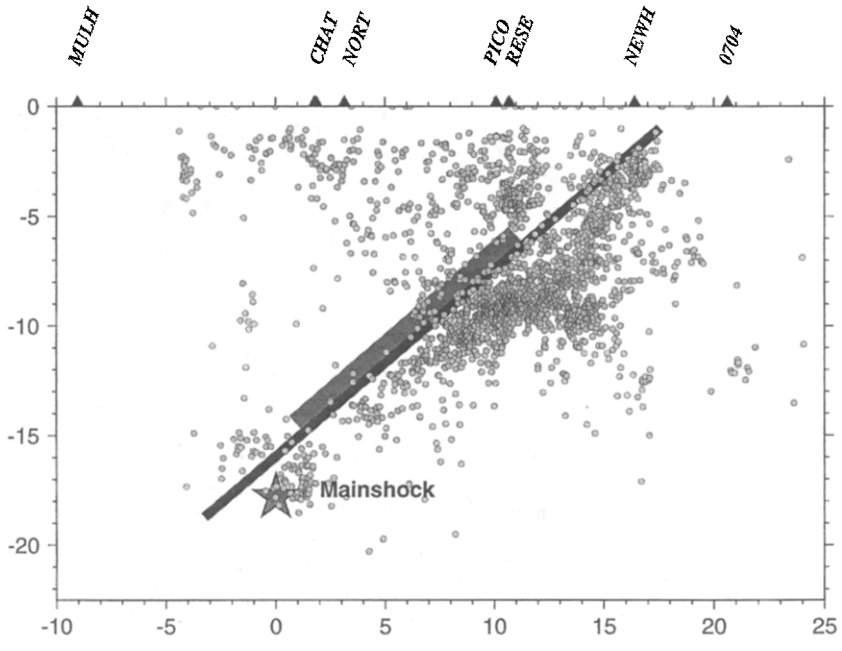

Figure 3. Cross section showing the model fault planes overlain on the aftershocks relocated by Mori *et al.* (1995). We find that one cannot model the geodetic data as well when assuming the fault plane is coplanar with the aftershocks. The uniform slip model plane is shown as a thick gray line, and the larger coplanar fault assumed for the variable slip model is shown as a thinner black line.

tions, obtaining a total moment of 1.63 × 10^{19} N-m and fitting the GPS data relatively well (χ^2 = 1681). Other solutions at higher and lower singular values yielded qualitatively similar slip distributions in the range $18 < k < 25$, where k is the number of singular values. Within this "stable" range, the total moment increased from 1.55 to 1.71 × 10^{19} N-m, and the data nrms decreased slightly. Although a more rigorous selection of the optimal result from this approach is possible using an F-test (Jacobsen and Shaw, 1991), we made our selection by inspection. It is valid, yet somewhat subjective, to select the number of singular values retained in this manner (e.g., Parker, 1977). Figure 4 shows the changes in key parameters with increasing number of singular values, allowing our selection to be evaluated. The additional parameter shown (subfault nrms) indicates dispersion in the amount of slip on each subfault.

As expected, the variable slip model does fit the data better than the uniform slip model, with a 40% reduction in variance. For this variable slip model (Fig. 5), we effectively estimated 23 parameters, whereas the uniform slip model has only 9. Taking this into account, we still find that the variable slip model (nrms = 3.10) fits the data better than does the uniform slip model (nrms = 3.32). Both models explain 95% or more of the variance, but neither provides a statistically satisfactory fit to the data. Using a less stringent norm, say by doubling all of the stated errors, one could claim that either model fits the data adequately, but we do not feel this would do justice to the problem. In one test, we doubled the stated vertical errors (but kept the horizontal errors the same) and reran the variable slip model. The result of this test, however, was a barely reduced total nrms within the "stable" range of singular values, at the expense of a considerably higher total moment and subfault nrms. That is, loosening the error constraints made the model less physically reasonable. For these reasons, we feel this issue requires discussion, as there are many possible sources of the misfit, and simply doubling the stated errors would not explain the recognized and suspected problems.

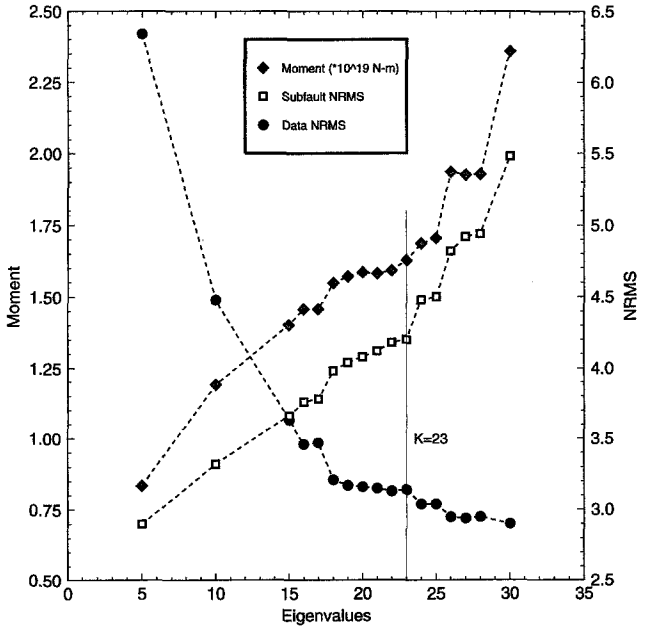

Figure 4. Total moment, subfault nrms, and data nrms (both based on reduced chi-squared values) as a function of the number of retained consecutive eigenvalues for the variable slip modeling. The total moment uses the length of each subfault's slip vector, summed over all subfaults. The subfault nrms is an index of dispersion for the length of all subfaults' slip vectors. The data nrms is a similar index for the model residuals.

Discussion

The normalized residuals between the data and either proposed model (Table 1 and Fig. 6) are greater than ex-

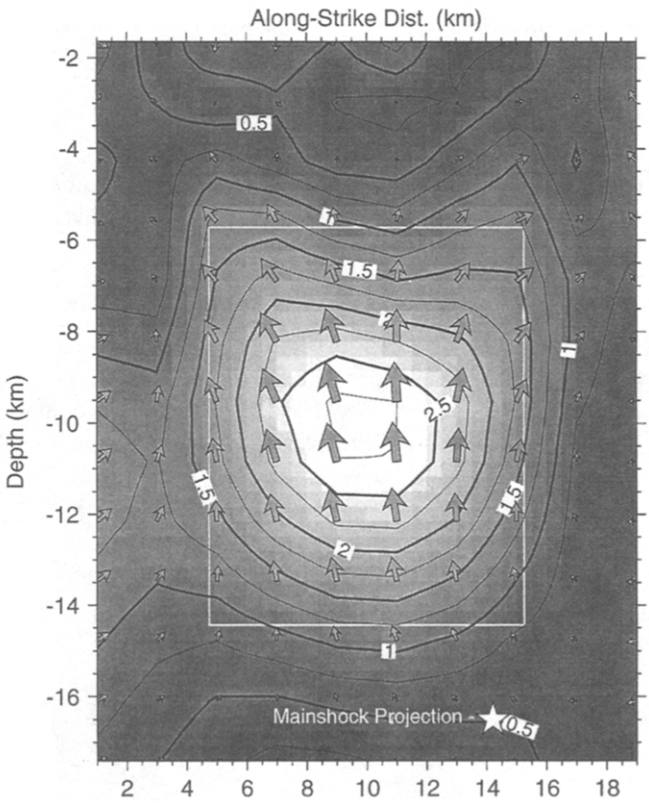

Figure 5. Distribution of slip on the Northridge fault plane. Contours and shading indicate the slip amplitude (in meters), and arrows indicate the slip vector for each subfault of the model. The model has 10 subfaults along-strike and 13 down-dip, each 2 by 2 km. Slip evidently occurred mainly up-dip and northwest of the hypocenter. Less than 1 m of slip occurred above a depth of 5 km. This model, based solely on the GPS data, differs substantially from those based solely on seismological data (Wald and Heaton, 1994b; Dreger, 1994). It differs, but less dramatically, with the "geodetic only" and "combined" models of Wald *et al.* (this issue).

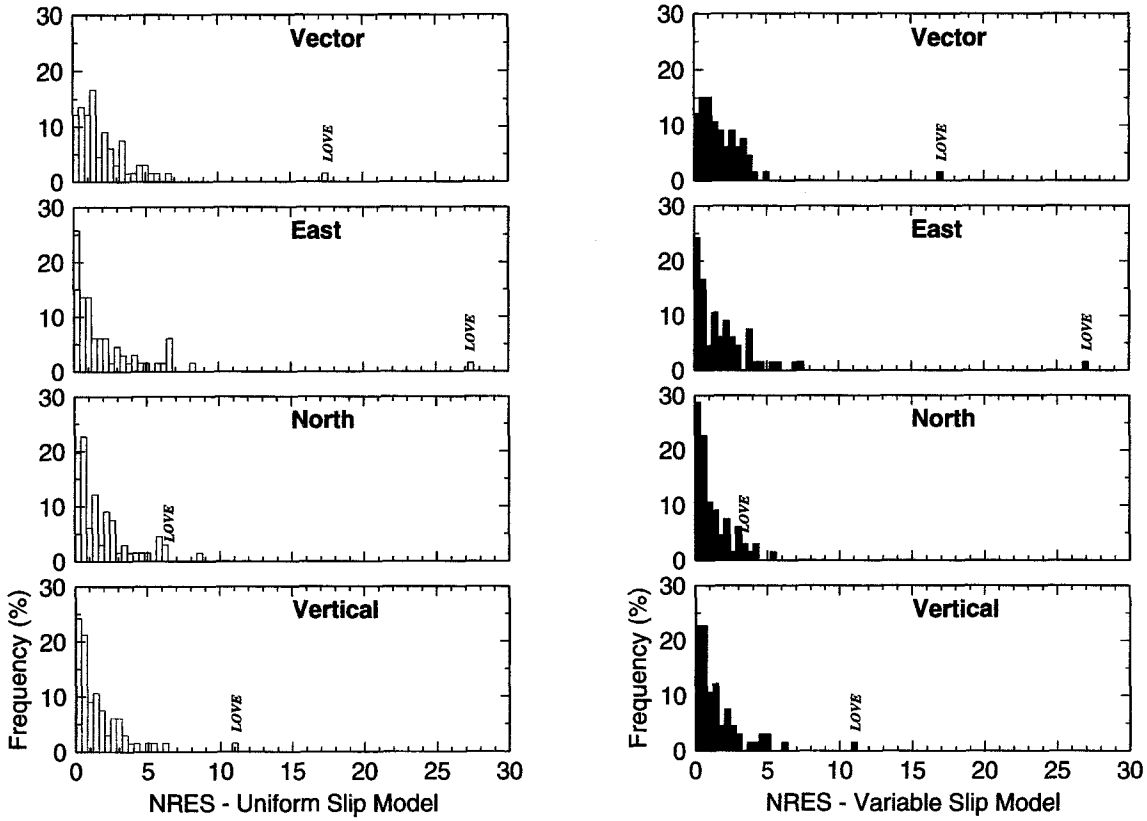

Figure 6. Distribution of normalized residual (NRES) values for the uniform and variable slip models. The outlier (especially in the east and vertical components) is station LOVE, whose displacement is anomalous (as discussed in the text).

pected (as is the summary nrms statistic for each model). This could be due in part to underestimating the measurement uncertainties, lack of an error model component representing monument instability, a poor physical model (i.e., neglecting the complexities of crustal structure and irregularities of the surfaces that ruptured, and the contributions of aftershocks), or data outliers (i.e., measurement blunders). Both modeling approaches have most difficulty fitting the same few stations, which are located within the same general area, so an inadequate physical model seems a likely explanation. However, the affects of aftershocks and monument instability may also be important for some stations.

Aftershocks. The displacement field contributions of aftershocks that occurred soon after the mainshock are, by necessity, included in our GPS data. Relatively shallow aftershocks, especially with $M > 5$, may have contributed to the displacement field we measured. For example, about 1 min after the mainshock, a shallow $M = 5.9$ aftershock occurred, and within 10 min, another shallow $M = 5.2$ occurred (according to the Caltech/USGS catalog based on Southern California Seismic Network data). Because these two events occurred so early after the mainshock, their locations and especially their depths are not well known. Hence, it is not possible to confidently model their contributions to the displacement field based solely on seismological information. In the preceding modeling section, we made no attempt to remove the effects of these two aftershocks, so what we call "co-seismic" actually includes these two early aftershocks. In that sense, our data differ from the seismological data used by Wald and Heaton (1994b) or Dreger (1994) to arrive at slip distribution models. Wald *et al.* (this issue) evaluate and discuss this issue.

Subsequent to these two early aftershocks, all other $M > 5$ aftershocks occurred between depths of 9 and 20 km, except for the shallow $M = 5.1$ event on 29 January. Displacement estimates given for the three GPS stations on Oat Mountain, PICO, SAFE, and SAFR are from data collected prior to the 29 January aftershock, and other GPS stations were unlikely to have been perturbed by that event. Over 40 aftershocks with $M > 4$ occurred within the first two weeks, many of which were shallow.

Monument Instability. Some errors may arise from infidelity of our survey monuments in representing tectonic signals. Although long-term monument stability is a serious issue for studies of interseismic motion, over the 16-month period of our observations, its effects are likely at the level of only a few millimeters (Langbein *et al.*, 1993a, 1993b; Wyatt, 1982; Johnson and Wyatt, 1994). More serious is the pos-

sibility that the strong shaking some of these monuments experienced during the Northridge earthquake may have created local displacements that are not representative of the upper crust.

Practices of surveying monument construction vary, as does the type of material in which monuments are emplaced. The simplest type of monument, several of which are used in this study, consists of a metal disk set with concrete into a drill hole in bedrock. Another common type consists of a concrete mass poured into a shallow hole that has been excavated in the soft rock or soil, with a metal disk at the top. Each of the older monuments used is one of these two types. More recently, for example, when Caltrans and NGS established the high precision geodetic network (HPGN) and HPGN-densification (HPGN-D) networks in the early 1990s, monuments called 3D rod marks were set in soft rock or soil. These marks are now preferred over the concrete mass type since they are not coupled to the uppermost soil and provide a deeper point of attachment to the ground. Still other monuments, of which there are few, are installed by attaching a metal disk to existing masonry such as retaining walls.

Because we typically have measured only one geodetic station at each location in our network, the contribution of monument instability to our errors is difficult to quantify. We have only one site (Oat Mountain) where coincidentally we had three separate monuments for which we obtained both pre- and postseismic GPS data of good quality. Also coincidentally, this site is the location of the largest displacements measured with GPS and presumably where ground shaking was very strong. The three Oat Mountain monuments (PICO, SAFE, and SAFR) are all set in soft, highly fractured rock capped with a thin (<0.5 m) veneer of soil. During the earthquake, these monuments likely experienced 0.5 to 1.0 g accelerations and 0.5 to 1.0 m/sec velocities. Monuments SAFE and SAFR are concrete masses with metal disks. From visual inspection before and after the earthquake, we concluded that SAFE was the better of the two because soil around the base of the concrete mass for SAFR had eroded away. PICO is a metal disk attached to a metal rod that was driven into the ground "to refusal" with a sledge hammer, and hence, it is probably less susceptible to surficial movements than either SAFE or SAFR. In Table 1, the results for motion of PICO, SAFE, and SAFR are given. The displacements estimated for these three sites disagree by up to 25 mm in the east component, up to 2 mm in the north component, and up to 28 mm in the vertical component. The differences in east and vertical displacements are outside our estimated 1-sigma measurement errors. These discrepancies occur between PICO and SAFE, the stations with better data. PICO was observed twice before and nine times after the earthquake, while SAFE was observed 10 times before and three times after (Fig. A1). SAFR has just one measurement each before and after the earthquake and is therefore suspect on geodetic grounds. We do not understand the discrepancy between our measurements at Oat Mountain, but we tentatively attribute them to localized monument instability induced by ground shaking in the earthquake. For this article, we have included the displacement estimates for PICO, SAFE, and SAFR in our modeling.

For another station, NORT, we had different concerns. The station is located about 3 km NNW of the mainshock epicenter; hence, its observed southeastward displacement is counterintuitive. The displacement was primarily vertical, with uplift of 213 ± 8 mm and horizontal motion of 68 ± 3 mm. This monument, an HPGN-D station, is a metal disk set in a poured concrete wall along a train track and flood control channel. The earthquake caused a train to derail adjacent to this station, and during the first occupations of this station after the event, we observed heavy equipment moving past the monument, within 1 m of the base of the wall. The equipment, which was being used to clear the train wreck from the tracks, compacted the asphalt road bed on the south side of the wall. When we arrived at the station, we observed a new crack in the wall (<10-mm movement), about 5 m southeast of the monument. The situation of the monument in such a wall, the crack that indicated damage to the structure, and the compaction of soil on the south side of the wall gave rise to concerns about monument instability. This monument was geodetically leveled before and after the earthquake relative to other benchmarks in the NGS/Caltrans vertical control network, and from this leveling, it appears that NORT went up by an amount similar to nearby benchmarks. We have no way to independently ascertain the horizontal integrity of the monument, except to say that by visual inspection, the wall appears to still be in line with the extension of the wall to the NW, and not to be tilted. In one test of the uniform slip model, the displacement of station NORT was left out without substantively changing the model results.

The station we have most difficulty fitting within errors is LOVE (Figs. 6 and 7). This station's displacement is very well determined, but the monument is a mass of concrete set in soft rock and soil. One possibility is that the motion of this monument included nontectonic motion induced by shaking since it also is located where strong ground motions occurred. There was a landslide and considerable ground cracking downhill from the site, but no cracks were observed north (uphill) of the site. A minor crack was observed to run in the soil through the monument. Although the assessment of those who visited the site was that the monument was probably not disturbed by more than 10 to 20 mm, the potential for significant nontectonic motion should not be overlooked.

The horizontal residual for NEWH is similar to that of LOVE, yet NEWH's residual is up (150 to 180 mm), whereas LOVE's residual is down (60 mm). Of course, since NEWH's displacement is less accurately determined, the modeling approaches we used would tend to allow its residual to be large. That is why we focus more on LOVE as the outlier station, even though the absolute residuals at NEWH are larger. The monument at NEWH is a concrete mass set in soil. Both NEWH and 0704 are very close to the up-dip displacement

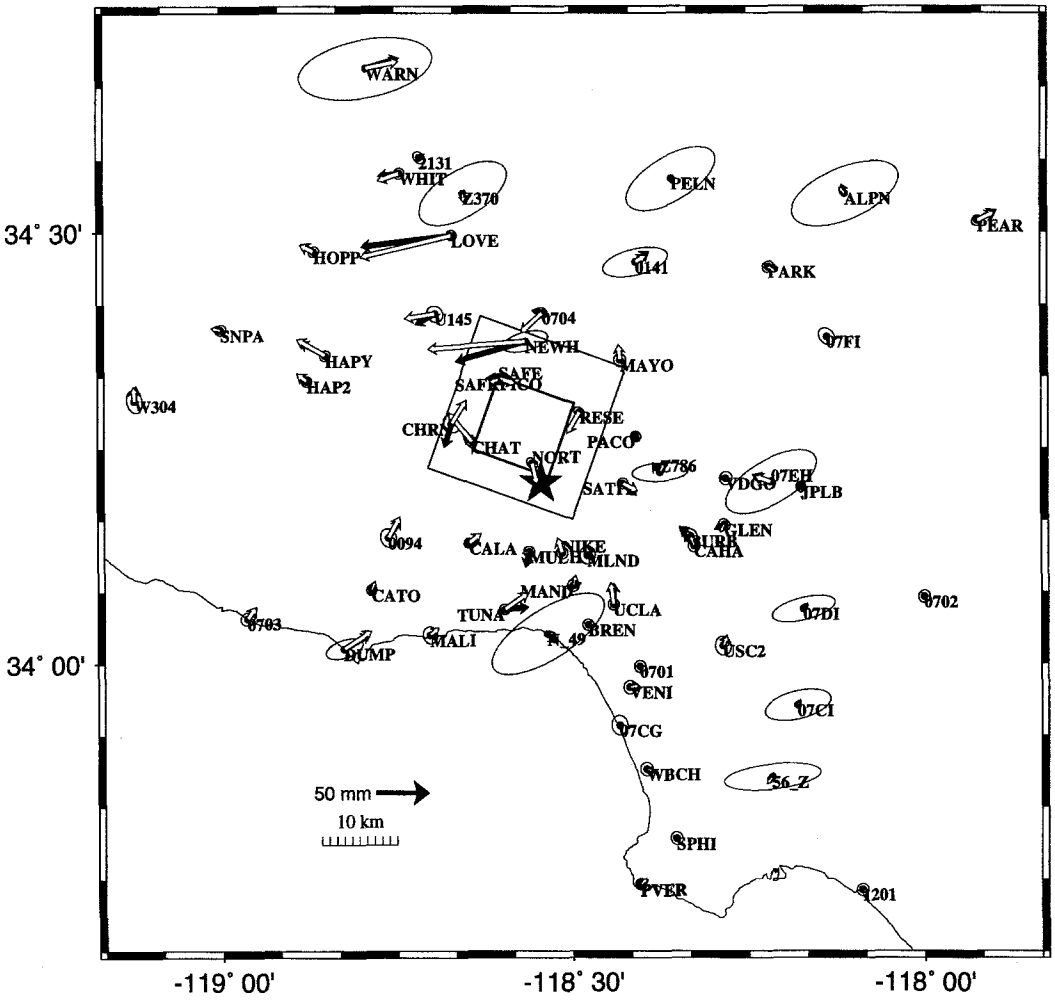

Figure 7. Residual vectors at the GPS stations. Some spatial systematics appear to remain in these unmodeled data, particularly in the vicinity of the eastern Ventura Basin, as discussed in the text. Also, residuals are significant but diversely oriented in the Santa Monica Mountains (near the down-dip edge of the rupture). Note the vector scale is several times larger than in Figure 1.

node, and we suspect that the misfits at these two stations may indicate some unmodeled slip on shallow structures (perhaps in combination with other potential problems we have mentioned). Aftershock seismicity indicates a steeper-dipping up-dip extension of the main rupture plane that would project to a line between these two stations, for example. Alternatively, the misfits could be explained by some sympathetic slip on hanging-wall structures.

Other stations in the vicinity of LOVE and NEWH (0704, CHAT, HAPY, HOPP, U145, and WHIT) are misfit less drastically, yet with a somewhat consistent westward component in the residual vectors (Fig. 7). Furthermore, preliminary results from leveling along highway 126 show unmodeled uplift of 10 to 20 mm in the vicinity of LOVE. We have considered the possibility that the misfits to data here may be due to seismic deformation associated with aftershocks, but we find it is not possible to account for the anomalies with the small displacement contributions of the aftershocks. An $M = 5.1$ aftershock that occurred on 19 January 1994 and located at a depth of 11 km was located close to these geodetic anomalies. This event had a pure reverse mechanism and is associated with seismicity on a north-dipping plane. The $M = 4.9$ aftershock on 26 June 1995 also occurred in this vicinity. If one postulates that some aseismic slip may have occurred on this north-dipping plane, it may be possible to improve fits to the geodetic data in the vicinity of stations LOVE and NEWH and along the highway 126 level line.

This apparently anomalous crustal deformation surrounds the intersection of the eastern Ventura Basin with the San Gabriel fault. It occurs in the area where the aftershocks most notably do not fall within the area of our model fault planes (Fig. 2). Furthermore, this area produced four preshocks $1.3 \leqq M \leqq 1.9$ at a depth of about 15 km within the 16 hr before the mainshock, called the Holser cluster (Hauksson *et al.*, 1995). It is not yet clear whether the prox-

imity of these preshocks and some larger aftershocks to the anomalous geodetic measurements is purely coincidental or may have a physical connection.

Fault Geometry and Material Properties

We are convinced from recent work on relocating the aftershocks by Mori *et al.* (1995) and Hauksson *et al.* (1995) that the fault geometry is more complicated than either a single uniform-slip dislocation or distributed slip on a single plane. Those studies indicate that the rupture almost surely occurred on a more complicated structure, so the geometry of our model is too simple. For example, the dip is shallower in the eastern portion of the aftershock zone than in the western portion. It is also possible that some shallow sympathetic slip may have occurred on a plane nearly parallel or perpendicular to the plane the mainshock occurred on, as suggested by south- and north-dipping features in the hanging-wall seismicity (Hauksson *et al.,* 1995). In addition, the seismicity indicates a somewhat deeper north-dipping structure near the northwestern up-dip corner of the rupture (closest to the anomalously displaced GPS stations U145, NEWH, and LOVE). The possibility of slip on other faults, particularly in the hanging wall, is investigated in Shen *et al.* (this issue). The geodetic data would be sensitive to even relatively small amounts of sympathetic slip on shallow structures, but future refinements of the modeling will be required to isolate any such affects. Geologists' formulations of the processes by which folds form (e.g., Suppe, 1985) include specific processes of localized deformation within the hanging wall; we do not attempt to take these into account here. Furthermore, we do not account for variable material properties within the earth's crust, and again, this may be a source of misfit. The challenge of adequately fitting our GPS results, perhaps with a more realistic fault geometry and/or more reasonable model of the crustal structure, remains to be met.

Preliminary Comparisons with Other Data

The pattern of uplift determined by extensive releveling (performed by the City of Los Angeles, National Geodetic Survey, and Caltrans) is roughly compatible with the models presented here. However, initial work with the leveling data has indicated that the total moment of our variable slip model is probably too high by about 20%. We also recognize that details of slip on the shallowest subfaults in the variable slip model presented here are not well resolved by the GPS data alone and that the leveling data will allow better imaging of the shallow slip. Furthermore, Murakami *et al.* (in press) have provided the first SAR interferometry results for the Northridge earthquake, and our variable slip model generally matches these independent data (although a lower total moment would also help us to match the SAR results better). We recognize at this stage that our uniform slip model is less consistent with either the leveling data or the SAR interferogram than is our variable slip model.

General Observations and Implications

The Northridge earthquake caused uplift of the Santa Susana Range, which seems intuitively sensible in terms of long-term displacement patterns. That is, the mountains, unsurprisingly, were pushed up by at least 400 mm (from our measurements at Oat Mountain), and perhaps as much as 520 mm (based on the maxima from our variable slip model). The largest amounts of uplift caused by the Northridge event fall along the crest of the Santa Susana range. More perplexing is our observation that the northern edge of the San Fernando Valley was also pushed up. It is difficult to reconcile this observation with the geomorphology of the area. The valley was pushed up less than the mountains, but nevertheless uplift of more than 200 mm occurred in Northridge, well south of the mountain front. Though we have only a few GPS stations within the San Fernando Valley that indicate uplift, preliminary releveling results show as much as 200 to 400 mm of uplift throughout the northern portion of the valley. Observed uplift of the northern San Fernando Valley qualitatively appears to conflict with the topography that has presumably been built, in large part, by prehistoric earthquakes.

The southward dip of the rupture plane in this event indicates that the fault is a backthrust, dipping contrary to the Sierra Madre fault system's orientation. The Oak Ridge fault system to the west also dips southward, implying that the Northridge earthquake occurred on an eastern extension of that fault system (e.g, Yeats, 1994). The Northridge fault plane, in turn, seems (from the aftershock seismicity) to be truncated at the upper edge by the fault that ruptured in the 1971 San Fernando (also known as Sylmar) earthquake (USGS and SCEC, 1994; Mori *et al.,* 1995). We appear to have imaged the up-dip truncation of slip at a depth of 4 to 6 km with our variable slip model (Figs. 3 and 5). This is slightly shallower than the intersection depth indicated by the seismicity. In places, the aftershocks extend spatially beyond the edges of the slip distribution model that we find best explains the geodetic data, especially near the northwest up-dip corner of the model fault (Figs. 2 and 3).

Slip in the Northridge earthquake was concentrated between depths of 5 and 20 km. Geologists have found no compelling evidence for a primary surface rupture (USGS and SCEC, 1994). Modeling indicates that in parts of the Santa Susana Range where we had no geodetic stations, uplift of as much as 520 mm may have occurred. In contrast, the 1971 earthquake, which was similar in magnitude, had large amounts of shallow slip and produced clear surface faulting (e.g., Heaton, 1982). As a result, the 1971 earthquake also produced much larger maximum displacements and commensurately larger strains and tilts at the ground surface (e.g., Savage *et al.,* 1975; Cline *et al.,* 1984). In that case, up to 2.5 m of vertical motion occurred over distances of 5 to 10 km, whereas the wavelength of vertical displacement associated with the Northridge event was several times longer as a result of the deeper concentration of large slip.

Conclusions

The displacement field of the earthquake was sampled by determining displacement vectors at 66 sites with respect to a time-dependent, well-established reference frame for global GPS tracking stations outside of southern California. The mean 1-sigma errors in these data are 8 mm (east–west), 6 mm (north–south), and 23 mm (vertical). From these precise measurements, we have quantified the displacement field associated with the Northridge earthquake (and its early aftershocks). The resulting data set, presented in Table 1, is of high quality and potentially high utility in understanding the earthquake. The data quality may, we hope, take others beyond the simple modeling efforts we have advanced in this article.

As a result of performing extensive analyses of the GPS data set, we feel that we understand the errors in the GPS data well enough to expect our models to fit these data appropriately within the stated errors, except for undetected problems at the less frequently measured stations. The exact reasons why our relatively simple models do not satisfactorily explain these GPS data remain unresolved, though we discuss the relevant issues and speculate that, perhaps most importantly, the source was too complex to be represented adequately with any single-plane model. The fact that we are not able to match the observations in a fairly well localized region to the north of the near-surface part of the fault plane suggests that the primary cause of the mismatch is using too simple a model, rather than monument instability.

From our GPS measurements, we produced a single-dislocation model independent of seismological and other information. Furthermore, the data were sufficient to allow an inversion in order to estimate the distribution of slip on the main fault plane. The observed displacement field was evidently produced mainly by slip on a SSW-dipping reverse fault in the mid-crust, under the northern edge of the San Fernando Valley. The Santa Susana Range was uplifted by the earthquake by as much as 400 mm (measured) to 520 mm (modeled), and the northern part of the San Fernando Valley was uplifted by more than 200 mm. The pattern of uplift caused by the Northridge earthquake appears discordant with the topography. Both of our modeling approaches indicate that in order to explain most of the variance in the GPS data, the largest amount of slip must have occurred up-dip and northwest of the event's hypocenter. We find that less than 1 m of slip occurred above a depth of about 5 km. We appear to have confirmed the suggestion by Mori *et al.* (1995) that the subsurface intersection with the 1971 earthquake fault plane formed the up-dip terminus of slip in the Northridge earthquake.

Our modeling indicates a simpler slip distribution than has been inferred on the basis of seismological data alone (Wald and Heaton, 1994b; Dreger, 1994). Clearly, the geodetic data and seismological data do not invoke identical images of the slip distribution. We present our variable slip model here partly to emphasize this point. Seismological data indicate slip concentrations near the down-dip edge of the rupture plane, whereas the geodetic data do not (see also; Wald *et al.,* this issue). This may be because there are too few GPS stations in the southern San Fernando Valley to resolve such features, or because contributions of these slip patches to the surface displacement field are too small to resolve with the available GPS data.

Geodetic data are well suited to mapping the final slip distribution of an earthquake and can therefore enhance imaging of rupture propagation beyond the capabilities of imaging based on seismological data alone, as was the case for the Landers earthquake (Hudnut *et al.,* 1994; Wald and Heaton, 1994a). By combining seismological and geodetic data, Wald *et al.* (this issue) attempt to resolve the differences noted above by using the combined seismological and geodetic data sets. It is also possible that the discrepancies seen result from aseismic slip; the geodetic measurements would include such phenomena, whereas the seismological data might not. Seismological and geodetic data are complementary, and combining the seismological data with geodetic data can provide the best available methods for imaging details of the earthquake source.

Acknowledgments

The GPS data used in this study were, in large part, collected through the cooperative efforts of several agencies and institutions. The National Geodetic Survey, Caltrans District 7 and Headquarters, Los Angeles County, and City of Los Angeles were the main surveying agencies that provided us with crucial assistance in GPS surveys conducted both prior to and following the Northridge earthquake. Without the work of these surveying agencies, only a portion of the results obtained in this study would have been possible. Of particular importance were the help of D. D'Onofrio, L. Fenske, R. Packard, R. Reader, and J. Satalich. The leveling results we discuss resulted from work by these agencies, in part supported by a FEMA mission assignment to the USGS under the direction of R. Stein. Also, the various field, logistical, and other efforts of many of our colleagues after the earthquake were greatly appreciated. We thank the following in particular: D. Agnew, J. Behr, E. Calais, K. Clark, M. Cline, G. Franklin, X. Ge, W. K. Gross, G. Hamilton, K. Hurst, D. Jackson, H. Johnson, S. Larsen, G. Lyzenga, D. Potter, M. Smith, J. Sutton, K. Stark, C. Stiffler, F. Webb, J. Zhang, and J. Zumberge. Much of the software used in producing, modeling, and displaying our results is freely available, and we particularly thank the developers of DISL, FONDA, GINV, GAMIT, GIPSY, GLOBK, and GMT who happen not to be co-authors of the present article: G. Blewitt, D. Dong, K. Feigl, K. Hurst, D. Jefferson, S. Larsen, W. Smith, F. Webb, P. Wessel, and J. Zumberge among many others. Though our published results were obtained using the GAMIT/GLOBK software, earlier analyses using FONDA and GIPSY/OASIS-II contributed significantly to the results. M. Murakami kindly provided a preprint of his article on the SAR interferometry results. We thank reviewers R. Stein, J. Mori, T. Heaton, and an anonymous reviewer for their suggestions. The National Earthquake Hazard Reduction Program (NEHRP) supported much of this work, both through the direct support of the USGS, NSF, and FEMA and indirectly through SCEC contracts with MIT, UCLA, and UCSD; portions of the research described in this work were carried out at the Jet Propulsion Laboratory, California Institute of Technology, under contract with NASA; research at UCSD is funded by Grants NASA NAG 5-1917, USGS 1434-92-G2196, NSF EAR 92 08447, and NSF EAR-9416338, as well as through SCEC. SCEC Contribution Number 153.

References

Beutler, G. and E. Brockmann (Editors) (1993). *Proc. of the 1993 IGS Workshop,* International Association of Geodesy, Druckerei der Universitat Bern.

Blewitt, G., Y. Bock, and G. Gendt (1993a). Regional clusters and distributed processing, *Proc. IGS Analysis Center Workshop,* J. Kouba (Editor), Int. Assoc. of Geodesy, Ottawa, Canada, 61–92.

Blewitt, G., M. Heflin, K. Hurst, D. Jefferson, F. Webb, and J. Zumberge (1993b). Absolute far-field displacements from the 28 June 1992 Landers earthquake sequence, *Nature* **361,** no. 6410 (28 January), 340–342.

Blewitt, G., Y. Bock, and G. Gendt (1995). Global GPS network densification: a distributed processing approach, *Man. Geod.,* in press.

Bock, Y., R. Abbot, C. Counselman, S. Gourevitch, and R. King (1986). Interferometric analysis of GPS phase observations, *Man. Geod.* **11,** 282–288.

Bock, Y., D. Agnew, P. Fang, J. Genrich, B. Hager, T. Herring, K. Hudnut, R. King, S. Larsen, J.-B. Minster, K. Stark, S. Wdowinski, and F. Wyatt (1993a). Detection of crustal deformation related to the Landers earthquake sequence using continuous geodetic measurements, *Nature* **361,** no. 6410 (28 January), 337–340.

Bock, Y., J. Zhang, P. Fang, J. Genrich, K. Stark, and S. Wdowinski (1993b). One year of daily satellite orbit and polar motion estimation for near real-time crustal deformation monitoring, in *Developments in Astrometry and Their Impact on Astrophysics and Geodynamics,* Kluwer Academic Publishers, Hingham, Massachusetts, 279–284.

Bock, Y., *et al.* (1995). Permanent GPS geodetic array in southern California: continuous monitoring of the crustal deformation cycle, *J. Geophys. Res.,* in preparation.

Chinnery, M. A. (1961). The deformation of the ground around surface faults, *Bull. Seism. Soc. Am.* **51,** 335–372.

Cline, M. W., R. A. Snay, and E. L. Timmerman (1984). Deformation of the earth model for the Los Angeles region, California, *Tectonophysics* **107,** 279–314.

Davis, T. L. and J. S. Namson (1994). A balanced cross-section analysis of the 1994 Northridge earthquake and thrust fault seismic hazards in southern California, *Nature,* in press.

Dong, D. (1993). The horizontal velocity field in southern California from a combination of terrestrial and space-geodetic data, *Ph.D. Dissertation,* Massachusetts Institute of Technology, 157 pp.

Donnellan, A., B. Hager, R. King, and T. Herring (1993a). Geodetic measurement of deformation in the Ventura Basin region, southern California, *J. Geophys. Res.* **98,** 21727–21739.

Donnellan, A., B. Hager, and R. King (1993b). Discrepancy between geological and geodetic deformation rates in the Ventura basin, *Nature* **366,** 333–336.

Draper, N. R. and H. Smith (1981). *Applied Regression Analysis,* Second Edition, 709 pp., Wiley, New York.

Dreger, D. S. (1994). Empirical Green's function study of the 17 January 1994 Northridge mainshock (M_w = 6.7), *Geophys. Res. Lett.* **21,** 2633–2636.

Ekstrom, G., R. Stein, J. Eaton, and D. Eberhart-Phillips (1992). Seismicity and geometry of a 110 km-long blind thrust fault, 1, The 1985 Kettleman Hills, Calif. earthquake, *J. Geophys. Res.* **97,** 4843–4864.

Fang, P., Y. Bock, J. F. Genrich, V. Otero, K. Stark, S. Wdowinshi, J. Zhang, T. A. Herring, and R. W. King (1992). Determination of precise satellite ephemerides, high-frequency earth rotation, and crustal deformation before and during the IGS Campaign, *EOS* **73,** 134.

Feigl, K., D. Agnew, Y. Bock, D. Dong, A. Donnellan, B. Hager, T. Herring, D. Jackson, T. Jordan, R. King, S. Larsen, K. Larson, M. Murray, Z. Shen, and F. Webb (1993). Space geodetic measurement of the velocity field of central and southern California, 1984–1992, *J. Geophys. Res.* **98 (B12),** 21677–21712.

Freymueller, J., N. E. King, and P. Segall (1994). The coseismic slip distribution of the Landers earthquake, *Bull. Seism. Soc. Am.* **84,** 646–659.

Hager, B. H., R. W. King, and M. H. Murray (1991). Measurement of crustal deformation using the global positioning system, *Annual Review of Earth and Planetary Sciences,* **19,** 351–382.

Harris, R. and P. Segall (1987). Detection of a locked zone at depth on the Parkfield segment of the San Andreas fault, *J. Geophys. Res.* **92,** 7945–7962.

Hauksson, E., L. Jones, and K. Hutton (1995). The 1994 Northridge earthquake sequence in Calif.: seismological and tectonic aspects, *J. Geophys. Res.,* in press.

Heaton, T. (1982). The 1971 San Fernando earthquake: a double event?, *Bull. Seism. Soc. Am.,* **72,** 2037–2062.

Herring, T. A. (1993). GLOBK: Global Kalman Filter VLBI and GPS analysis program, v. 3.1, Massachusetts Institute of Technology, Cambridge, 1993.

Hudnut, K. W. and M. H. Murray (1994). The Northridge earthquake—preliminary GPS results of the USGS; IGS E-Mail #0466; http://igscb.jpl.nasa.gov/igscb/mail/igsmail/igsmess.466.

Hudnut, K. W., Y. Bock, M. Cline, P. Fang, Y. Feng, J. Freymueller, X. Ge, K. Gross, D. Jackson, M. Kim, N. King, J. Langbein, S. Larsen, M. Lisowski, Z. Shen, J. Svarc, and J. Zhang (1994). Co-seismic displacements of the 1992 Landers earthquake sequence, *Bull. Seism. Soc. Am.* **84,** 625–645.

Hudnut, K. W. and S. C. Larsen (1993). Slip distribution in the Landers, Calif., earthquake sequence determined from geodetic data, *EOS* **74,** no. 43, 183 (submitted to JGR).

Jackson, D. D. (1972). Interpretation of inaccurate, insufficient, and inconsistent data, *Geophys. J. R. Astr. Soc.* **28,** 97–107.

Jacobsen, R. S. and P. R. Shaw (1991). Using the F-test for eigenvalue decomposition problems to find the statistically "optimal" solution, *Geophys. Res. Lett.* **18,** no. 6, 1075–1078.

Johnson, H. O. and F. Wyatt (1994). Geodetic network design for fault-mechanics studies, *Manuscripta Geodaetica,* in press.

King, R. W. and Y. Bock (1994). Documentation of the GAMIT GPS analysis software v. 9.3, Massachusetts Institute of Technology and Scripps Institute of Oceanography.

Langbein, J., D. Hill, T. Parker, and S. Wilkinson (1993a). An episode of reinflation of the Long Valley Caldera, Eastern California—1989–1991, *J. Geophys. Res.* **98,** 15851–15870.

Langbein, J., E. Quilty, and K. Breckenridge (1993b). Sensitivity of crustal deformation instruments to changes in secular rate, *Geophys. Res. Lett.* **20,** no. 2, 85–88.

Larsen, S. C. (1991). Geodetic measurements of deformation in southern California, *Ph.D. Dissertation,* California Institute of Technology, Pasadena, 351 pp.

Mansinha, L. and D. E. Smylie (1971). The displacement fields of inclined faults, *Bull. Seism. Soc. Am.* **61,** 1433–1440.

Menke, W. (1989). *Geophysical Data Analysis: Discrete Inverse Theory,* vol. 45, Int'l. Geophys. Series, Academic Press, Inc., San Diego.

Mori, J., D. J. Wald, and R. L. Wesson (1995). Overlapping fault planes of the 1971 San Fernando and 1994 Northridge, California earthquake, *Geophys. Res. Lett.* **22,** no. 9, 1033–1036.

Murakami, M., M. Tobita, S. Fujiwara, T. Saito, and H. Masaharu. Coseismic crustal deformations of the 1994 Northridge California earthquake detected by interferometric JERS-1 SAR, *J. Geophys. Res.,* in press.

Murray, M. H., G. A. Marshall, M. Lisowski, and R. S. Stein (1994). The 1992 M=7 Cape Mendocino, California earthquake: coseismic deformation at the southern end of the Cascadia megathrust, *J. Geophys. Res.,* submitted.

Okada, Y. (1985). Surface deformation due to shear and tensile faults in a half-space, *Bull. Seism. Soc. Am.* **75,** 1135–1154.

Parker, R. L. (1977). Understanding inverse theory, *Ann. Rev. Earth Planet. Sci.* **5,** 35–64.

Savage, J. and L. Hastie (1966). Surface deformation associated with dip-slip faulting, *J. Geophys. Res.* **71,** 4897–4904.

Savage, J. C., R. O. Burford, and W. T. Kinoshita (1975). Earth movements from geodetic measurements, in San Fernando, Calif., earthquake of

9 February 1971, G. B. Oakeshott (Editor), *Calif. Div. Mines Geol. Bull.* **196,** 175–186.

Segall, P. and R. Harris (1987). Earthquake deformation cycle on the San Andreas fault near Parkfield, California, *J. Geophys. Res.* **92,** 10511–10525.

Shen, Z.-K., X. Ge, D. Jackson, D. Potter, M. Cline, and L. Sung (1996). Northridge earthquake rupture models based on GPS measurements, *Bull. Seism. Soc. Am.* **85.**

Steketee, J. A. (1958). Some geophysical applications of the elasticity theory of dislocations, *Can. J. Phys.* **36,** 1168–1198.

Stein, R. and G. Ekstrom (1992). Seismicity and geometry of a 110 km-long blind thrust fault, 2, Synthesis of the 1982–1985 Calif. earthquake sequence, *J. Geophys. Res.* **97,** 4865–4883.

Stein, R. S., G. C. P. King, and J. Lin (1994). Stress triggering of the 1994 M = 6.7 Northridge, Calif. earthquake by its predecessors, *Science* **265,** 1432–1435.

Suppe, J. (1985). *Principles of Structural Geology,* 537 pp., Prentice-Hall, Englewood Cliffs, New Jersey.

USGS and SCEC Scientists (1994). The magnitude 6.7 Northridge, Calif. earthquake of January 17, 1994, *Science* **266,** 389–397.

Wald, D. J. and T. H. Heaton (1994a). Spatial and temporal distribution of slip for the 1992 Landers, California, earthquake, *Bull. Seism. Soc. Am.* **84,** 668–691.

Wald, D. J. and T. H. Heaton (1994b). A dislocation model of the 1994 Northridge, CA, earthquake determined from strong ground motions, *U.S. Geol. Surv. Open-File Rep. #94-278.*

Wald, D. J., T. H. Heaton, and K. W. Hudnut (1996). The slip history of the 1994 Northridge, California, earthquake determined from strong-motion, teleseismic, GPS, and leveling data, *Bull. Seism. Soc. Am.* **86,** no. 1B, S49–S70.

Webb, F. H. and J. F. Zumberge (1993). An introduction to GIPSY/OASIS-II, JPL D-11088, Jet Propulsion Lab.

Wessel, P. and W. H. F. Smith (1991). Free software helps map and display data, *EOS* **72,** no. 441, 445–446.

Wyatt, F. (1982). Displacements of surface monuments: horizontal motion, *J. Geophys. Res.* **87,** 979–989.

Yeats, R. S. (1994). Oak Ridge fault system and the 1994 Northridge, California, earthquake, *Nature,* in press.

Zhang, J., Y. Bock, P. Fang, J. Behr, J. Genrich, and K. Hudnut (1994). Surface deformation in the Northridge earthquake and the Los Angeles Basin from the PGGA time series, *EOS,* **75,** no. 44, 166.

Zumberge, J. F., G. Blewitt, M. B. Heflin, D. C. Jefferson, and F. H. Webb (1992). Analysis procedures and results from the 1992 IGS Campaign (abstract), *EOS* **73,** 134.

U.S. Geological Survey
525 South Wilson Ave.
Pasadena, California 91106
(K. H.)

Department of Earth and Space Sciences
University of California, Los Angeles
Los Angeles, California 90024
(Z.-K.S., Y.F.)

U.S. Geological Survey
345 Middlefield Rd., MS #977
Menlo Park, California 94025
(M.M.)

Department of Earth, Atmospheric, and Planetary Sciences
Massachusetts Institute of Technology
Cambridge, Massachusetts 02146
(S.M., R.K., T.H., B.H.)

Institute of Geophysics and Planetary Physics
Scripps Institution of Oceanography
UCSD
La Jolla, California 92093
(Y.B., P.F.)

Jet Propulsion Laboratory
MS 238-600
4800 Oak Grove Drive
Pasadena, California 91109-8099
(A.D.)

Manuscript received 17 January 1995.

Table A1
GPS Station Information

Station ID	Approximate Location: Latitude (north)	Longitude (west)	Elevation (m)	*A Priori* Velocities (ITRF 93): East (mm/yr)	North (mm/yr)	Up (mm/yr)	Monument Information: Station Designation and Stamping	Station Aliases	NGS ID
0094	34.1464	118.7610	271	−48.4	13.1	0.3	CADT GPS 0094 1992		
0141	34.4654	118.4073	553	−40.7	8.7	4.1	LACFCD 145-02390 1964		EW2709
0618	34.8252	118.8681	1111	−31.1	2.8	5.1	HPGN CA 06 18		EW9546
0701	33.9965	118.4033	10	−47.2	13.3	−0.3	HPGN CA 07 01		DY9308
0702	34.0776	117.9995	99	−41.9	8.5	1.3	HPGN CA 07 02		EV9239
0703	34.0528	118.9627	11	−49.8	13.5	0.3	HPGN CA 07 03		EW9547
0704	34.4071	118.5401	357	−43.5	9.4	4.4	HPGN CA 07 04		EW9548
0705	34.4927	118.7651	1062	−30.4	0.6	1.7	HPGN CA 07 05		EV9240
07CG	33.9282	118.4329	24	−47.5	13.4	−0.3	HPGN-D 07-CG VEN 1-9G	0158	
07CI	33.9513	118.1798	34	−44.2	9.2	1.6	07-CI HPGN-D 1992 (3-D-ROD)	0155	
07DI	34.0632	118.1711	136	−43.2	8.8	1.6	HPGN-D 07-DI 1992 (3-D ROD)	0153	
07EH	34.2107	118.2158	444	−42.1	8.1	1.6	07-EH HPGN CALIF-D 1992	0147	
07FI	34.3794	118.1362	1775	−38.6	6.4	1.3	07-FI (BOLT)	0142	
1201	33.7375	118.0883	8	−46.3	14.0	−0.8	HPGN CA 12 01		DY9309
2131	34.5859	118.7141	860	−41.1	5.6	−3.0	213-128 1974 RE 7078	213-128	
56_Z	33.8682	118.2160	17	−46.4	13.7	−0.5	MWDSC 56 Z 1933	0159	
ALPN	34.5436	118.1092	864	−33.6	3.1	1.7	ALPINE 1938	0024	EW0229
BREN	34.0447	118.4765	90	−47.0	13.7	−0.3	BRENTWOOD ECC. 6	SAW D-7, BREN, 0190	
BURB	34.1479	118.3309	157	−43.9	8.4	1.9	BURBANK 1953 1-7	0148	
CAHA	34.1370	118.3258	524	−43.9	8.5	1.9	CAHUENGA #2 1933	BUR J-8, 0280	
CALA	34.1401	118.6457	497	−47.7	13.2	0.2	CALABASAS 1933 RE 62	DC G-8, 0087, 0240	EW7450
CATO	34.0858	118.7858	826	−48.6	13.4	0.2	SOLSTICE CYN B.2 AUX 1 1966	CASTRO PEAK	
CHAT	34.2571	118.6406	674	−46.6	10.4	4.3	CHATSWORTH 1924	CHA H-6, 0330	
CHRN	34.2788	118.6702	381	−46.8	10.4	4.4	COCHRAN 1975	0115	EW7403
DUMP	34.0176	118.8248	7	−48.9	13.6	0.2	DUME PT. J-10 1950 RE 329	6024	EW4188
GLEN	34.1612	118.2826	107	−43.2	8.4	1.8	BE 102 USE	0102, BE10	
HAP2	34.3280	118.8771	332	−45.3	13.2	−2.8	HAPPY 2 1992	0113	
HAPY	34.3580	118.8501	704	−45.0	13.0	−2.7	HAPPY 1959		
HOPP	34.4777	118.8655	1345	−42.2	7.6	4.8	HOPPER 1941		
JPLM	34.2048	118.1732	450	−41.8	8.2	1.5	JPL MV-3 1983 CDP 7272 (PERMANENT)	IERS 40400 M006/M007, JPL1	
LOVE	34.4963	118.6687	727	−42.7	6.2	−3.1	LOMA VERDE RESET 1961		
MALI	34.0332	118.7019	59	−48.3	13.6	0.1	CADT MALIBU 1992	6022	
MAND	34.0905	118.4982	448	−46.9	13.5	−0.2	MANDEVILLE 1933	SAW A-2, 0255	
MAYO	34.3522	118.4296	1173	−43.0	9.8	3.9	MAY 1932	SYL I-6, 0370	
MLND	34.1259	118.4769	364	−46.1	11.2	3.6	CADT MULHOLLAND 1992 (3-D ROD)	6004	
MULH	34.1301	118.5599	475	−47.2	13.3	0.0	13-F-21 1940	13F2	
NEWH	34.3742	118.5638	365	−44.2	9.7	4.5	NEWHALL SURVEYS 1993	0353	
NIKE	34.1288	118.5129	569	−46.3	11.1	3.7	NIKE RESET 1978	RES K-9A, 0260	
NORT	34.2328	118.5552	262	−46.0	10.6	4.0	NORTHRIDGE LS 6172 1992	6003	
N_49	34.0343	118.5340	6	−47.3	13.7	−0.2	LAC N 49	6012	
OJAI	34.4399	119.2022	335	−47.9	9.2	−4.7	CADT OJAI 1992	0106	
PACO	34.2636	118.4083	393	−43.9	10.6	3.6	PACOIMA #2 LAC C 1933	PAC L-5, 0144, 0350	EW7328
PARK	34.4598	118.2188	1259	−37.7	5.5	1.7	PARKER J-5 1989 RE 11915	0022	EW7208
PEAR	34.5121	117.9224	924	−31.8	1.9	1.7	PEARBLOSSOM NCMN 7254 1983	6073, 5001, 0061	DZ1220
PELN	34.5610	118.3561	1479	−36.7	4.4	−3.8	PELONA 1932	0019, PELO	EW7132
PICO	34.3306	118.6013	1102	−45.4	10.0	4.4	PICO NCER 1977 USGS		
PVEP	33.7433	118.4042	70	−47.6	13.9	−0.4	PVEP (UNSTAMPED) (PERMANENT)	IERS 40403 M002	
PVER	33.7438	118.4036	106	−47.6	13.9	−0.4	PALOS VERDES ARIES 7268 1976 1980	PALO, 1000, 6002	DY9148
RESE	34.2917	118.4882	395	−44.5	10.3	4.0	RESERVOIR 1932	0015	EW7332
SAFE	34.3304	118.6013	1103	−45.4	10.0	4.4	PICO L9C	SAN FERNANDO	
SAFR	34.3305	118.6014	1103	−45.4	10.0	4.4	AUX.2 ECC.1 RM.2 1967 RE 5869	AUX2	
SATI	34.2092	118.4264	218	−44.8	10.9	3.6	SATICOY (UNSTAMPED)	5004, 0+00 SATICOY B.L.	
SNPA	34.3879	118.9988	200	−46.8	10.4	2.0	SANTA PAULA NCMN 7255 1981	SANT	
SPHI	33.7968	118.3525	140	−47.3	13.8	−0.4	SAN PEDRO HILLS J-1	0040, 6007	DY2861

Table A1
Continued

Station ID	Approximate Location: Latitude (north)	Longitude (west)	Elevation (m)	*A Priori* Velocities (ITRF 93): East (mm/yr)	North (mm/yr)	Up (mm/yr)	Monument Information: Station Designation and Stamping	Station Aliases	NGS ID
TUNA	34.0630	118.5955	538	−47.6	13.6	−0.1	TUNA 1933	TC A-5, 0210	
U145	34.4059	118.6929	262	−44.9	6.9	−3.2	U 1451 1989 (3-D ROD)	0109	EW9447
UCLA	34.0687	118.4410	200	−45.6	8.6	2.1	UCLA, YOUNG HALL ROOF		
USC2	34.0203	118.2853	21	−44.6	8.9	1.8	USC (UNSTAMPED)		
VDGO	34.2151	118.2801	931	−42.6	8.1	1.8	VERDUGO ECC. 1	LCR C-11A, 0310	
VENI	33.9722	118.4186	14	−47.4	13.3	−0.3	VENICE K-4C	5006	
W304	34.3058	119.1233	24	−48.3	11.0	1.8	W 304 1934	0110	
WARN	34.6877	118.7903	806	−38.7	4.8	−3.2	WARNE 1992	6028	
WBCH	33.8773	118.3945	72	−47.5	13.6	−0.4	TORRANCE E-3 ECC 7	0090, 6006	DY2915
WHIT	34.5674	118.7428	700	−41.9	6.0	−3.0	WHITAKER PK AUX NO 1 NO 3 1964 A-7A		
Z370	34.5445	118.6517	658	−41.4	5.8	−3.0	Z 370 1953 RESET 1967	6026	EW2774
Z786	34.2223	118.3734	252	−43.4	8.0	2.1	Z-786 1946	0146	EW2127

Table A2
GPS Data Sets (Experiments) Used in This Study

Survey Name	Identity	Time	Type	Length	Lead Agencies
Pre-earthquake:					
HPGN-Densification	HPGN-D2	Oct. 1992	TR-C[1]/P[2]	2–6 hr.	Caltrans/NGS
Inter-County	IC'93	July 1993	TR/AS[3]	6 hr.	USGS/SCEC
Partial HPGN-D net	HPGN-D3	Oct. 1993	TR-C[1]/P[2]	2–6 hr.	Caltrans
Ventura Basin	VB'93	Nov. 1993	OS-TR[4]	24+ hr.	JPL/MIT
Post-earthquake:					
Earthquake response	EQ'94	Jan. 1994	TR/AS[5]	6–24+ hr.	USGS/SCEC
HPGN and HPGN-D	COOP'94	Feb. 1994	TR-C/P[6]	2–6 hr.	Caltrans/NGS
Continuous:	PGGA	all above	TR-P[2], AS[5],	OS-TR[4]	UCSD/JPL

*TR-C refers to Trimble 4000 SST model receivers: dual-frequency L2-codeless. Geodetic control purposes to NGS first-order "group B" specifications.

†TR-P refers to Trimble 4000 SSE model receivers: dual-frequency P-code. Geodetic control purposes to NGS first-order "group C" specifications.

‡The Inter-County 1993 survey used a mix of TR-C/P and Ashtech (AS) C/P receivers.

§OS-TR refers to Osborne TurboRogue model receivers: dual-frequency P-code.

‖The earthquake response surveys within the first few weeks used a mix of TR-C/P, OS-TR, and AS-C/P receivers. Stations of the HPGN, HPGN-D, IC, and VB nets were occupied. This was a cooperative effort of scientists represented in this article, many of whom are listed in the acknowledgments.

¶The HPGN and HPGN-D network stations within a radius of about 75 km of the mainshock were surveyed in mid-February 1994, cooperatively with local government agencies and SCEC.

References:

October/November 1992—Caltrans HPGN-D. Supervised by Jay Satalich, Caltrans District 7. Processed by UCLA and USGS.

July, 1993—USGS/SCEC Inter-County Survey. Organized by Ken Hudnut, USGS. Processed by UCLA, MIT, USGS.

October 1993—Caltrans HPGN-D partial survey. Supervised by Jay Satalich, Caltrans District 7. Processed by UCLA and USGS.

November 1993—JPL/MIT Ventura Basin Survey (Donnellan *et al.,* 1993a, 1993b). Organized by Andrea Donnellan, JPL. Processed by MIT and JPL.

January/February 1994—USGS/UCLA/JPL/MIT/UCSD postearthquake response surveys (Hudnut *et al.,* 1994). Organized by Ken Hudnut, USGS (IC and HPGN/HPGN-D stations) and Andrea Donnellan, JPL (VB stations). Processed by JPL (VB stations), UCLA (all stations), USGS (all), and MIT (all).

February 1994—Caltrans/NGS cooperative post-earthquake survey. Organized by Don D'Onofrio, NGS and Jay Satalich, Caltrans District 7. Processed by UCLA and MIT.

All of the global and regional GAMIT tracking solutions were produced by UCSD (Fang *et al.,* 1992) and all of those for GIPSY were produced by JPL (Zumberge *et al.,* 1992).

Software used in these data analyses included FONDA (Dong, 1993), GAMIT (King and Bock, 1994), GIPSY/OASIS-II (Blewitt *et al.,* 1993b, Webb and Zumberge, 1993), and GLOBK (Herring, 1993).

Acronym Key:

California Division of Transportation (Caltrans), National Geodetic Survey (NGS), Jet Propulsion Lab (JPL), Massachusetts Institute of Technology (MIT), University of California, Los Angeles (UCLA), Scripps Institute at University of California, San Diego (Scripps/UCSD), and Southern California Earthquake Center (SCEC)—in some places representing contributions of all collaborating universities (MIT, UCLA, UCSD) as well as JPL.

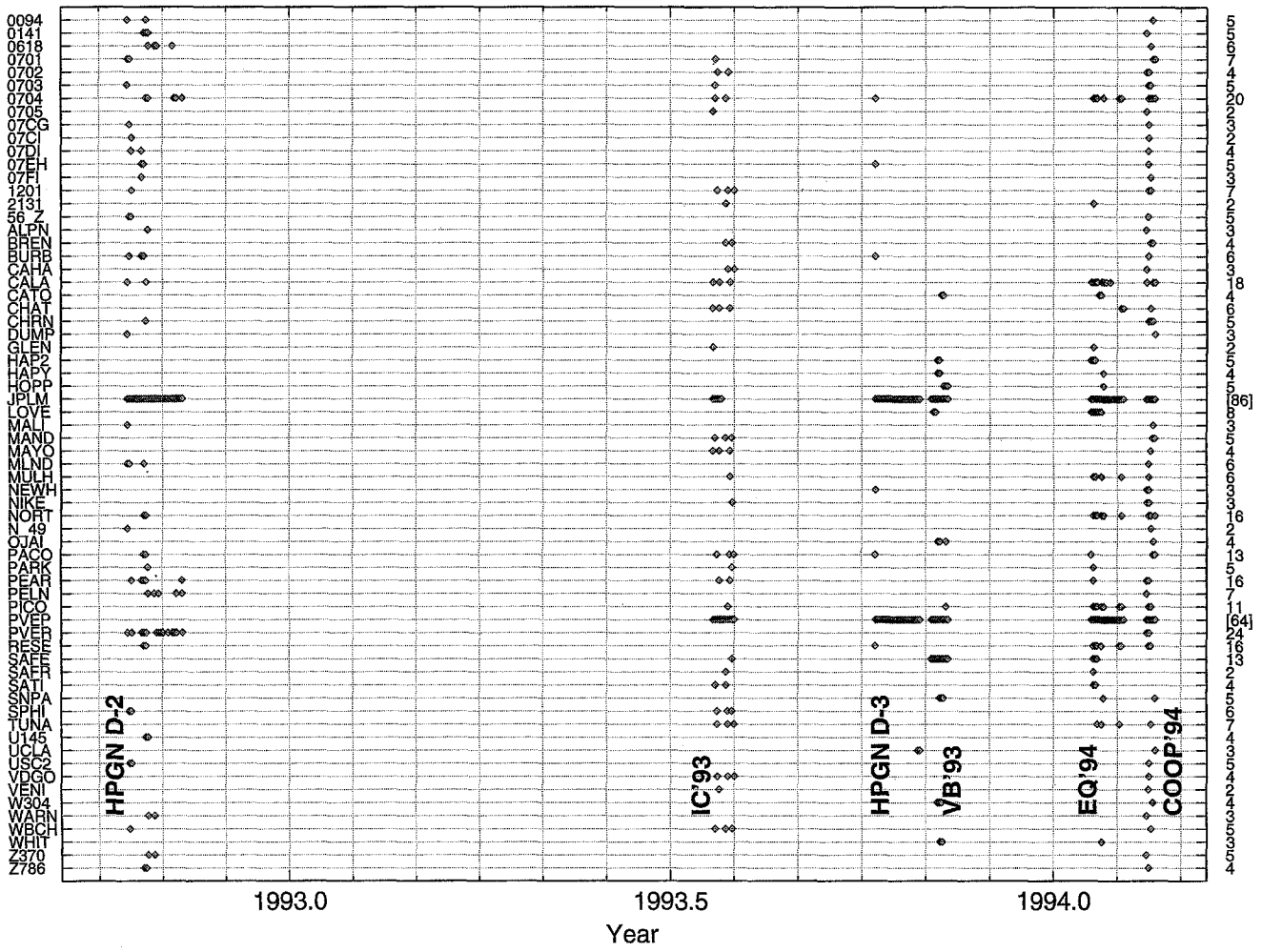

Figure A1. GPS station history of occupations. Station names are given on the left, and the total number of occupations for each station is given on the right. Each occupation is shown as a diamond symbol (except that in the Caltrans/NGS surveys; multiple sessions on the same day are represented by one symbol). Stations with a total of only two or three occupations are most susceptible to coarse errors.